Russian Physics Journal, Vol. 53, No. 9, 2011

PATTERN-FORMING CIRCUIT FOR AN ULTRA-WIDEBAND MULTIBEAM ANTENNA ARRAY

Yu. I. Buyanov, V. I. Koshelev, and P. F. Shvadlenko UDC 621.396.677.49

In the present work, the possibility of developing a pattern-forming circuit for an ultra-wideband multibeam antenna array is studied. Results of investigations of separate elements of the pattern-forming circuit are presented. Brief analytical calculation of an ultra-wideband directional coupler is presented together with calculation procedure and characteristics of the pattern-forming circuit for a four-beam antenna array. Results of calculations and measurements of the characteristics of the directional coupler are presented. A variant of the topology of the pattern-forming circuit is suggested.

Keywords: ultra-wideband antenna array, pattern-forming circuit.

INTRODUCTION

In the development of radio systems using ultra-wideband (UWB) nanosecond and subnanosecond pulses, a problem arises of control over the spatial beam position in real time. This problem can be solved through the development of UWB multibeam antenna arrays (MAA) representing an antenna system having several inputs each with a specific amplitude-phase distribution over the array aperture. The MAA are widely used in narrow-band systems and have been investigated in sufficient detail. The multibeam arrays have M inputs, N transmitters, and a pattern-forming circuit (a matrix) that allows up to M beams to be transmitted simultaneously and independently. When all inputs operate simultaneously, M independent beams are transmitted, and when the inputs operate successively, one beam corresponding to the connected input is transmitted.

Two main MAA types based on the Blass and Butler matrices are well known [1]. One of the variants is the Nolen matrix representing a combination of the Blass and Butler matrices. For transmission or reception of UWB signals, only the Blass matrix and its modifications providing the position of the pattern maximum independent of the frequency can be used. In the last few years, the MAA with extended bandwidth have been reported in [2, 3]. As a rule, their bandwidths did not exceed one octave, whereas 2–3 octaves were required for efficient transmission and reception of UWB pulses. In this regard, studies of the possibility of developing the MAA with bandwidths significantly exceeding one octave and elucidation of the mechanisms distorting the UWB pulse shapes are of interest.

ULTRA-WIDEBAND MULTIBEAM ANTENNA ARRAYS

The pattern-forming circuit (PFC) of the multibeam antenna array based on the Blass matrix is shown in Fig. 1. The PFC has M inputs (channels) and N outputs (transmitters) and comprises two systems of mutually crossed feeder lines coupled with each other in places of crossing with the help of directional couplers.

Each directional coupler (DC) is characterized by its own parameters: coupling coefficient $R \cdot \exp(i\varphi)$ and transmission coefficient $T \cdot \exp(i\psi)$. To analyze the PFC, we now consider a four-beam MAA with four transmitters

Institute of High-Current Electronics of the Siberian Branch of the Russian Academy of Sciences, Tomsk, Russia, e-mail: yurbuy@yandex.ru; spf@lhfe.hcei.tsc.ru. Translated from Izvestiya Vysshikh Uchebnykh Zavedenii, Fizika, No. 9, pp. 5–9, September, 2010. Original article submitted June 24, 2010.

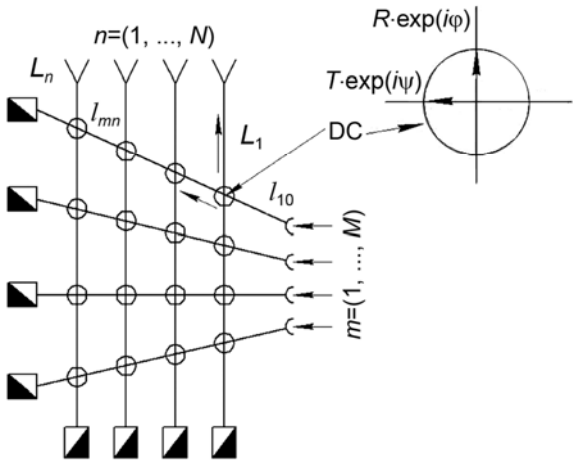

Fig. 1. Block diagram of the multibeam antenna array based on the Blass matrix.

and four inputs. The amplitude distribution for the transmitters corresponding to each of the M channels having identical directional couplers can be described by the following expressions [4]:

1st channel

$$\begin{cases} R\cdot\exp[i\gamma(l_{11})]\exp[i(\varphi)], \\ TR\cdot\exp[i\gamma(l_{12})]\exp[i(\varphi+\psi)], \\ T^2R\cdot\exp[i\gamma(l_{13})]\exp[i(\varphi+2\psi)], \\ T^3R\cdot\exp[i\gamma(l_{14})]\exp[i(\varphi+3\psi)], \end{cases}$$

2nd channel

$$\begin{cases} TR\cdot\exp[i\gamma(l_{11}+l_{21})]\exp[i(\varphi+\psi)], \\ T^2R\cdot\exp[i\gamma(l_{12}+l_{22})]\exp[i(\varphi+2\psi)], \\ T^3R\cdot\exp[i\gamma(l_{13}+l_{23})]\exp[i(\varphi+3\psi)], \\ T^4R\cdot\exp[i\gamma(l_{14}+l_{24})]\exp[i(\varphi+4\psi)], \end{cases}$$

3rd channel

$$\begin{cases} T^2R\cdot\exp[i\gamma(l_{11}+l_{21}+l_{31})]\exp[i(\varphi+2\psi)], \\ T^3R\cdot\exp[i\gamma(l_{12}+l_{22}+l_{32})]\exp[i(\varphi+3\psi)], \\ T^4R\cdot\exp[i\gamma(l_{13}+l_{23}+l_{33})]\exp[i(\varphi+4\psi)], \\ T^5R\cdot\exp[i\gamma(l_{14}+l_{24}+l_{34})]\exp[i(\varphi+5\psi)], \end{cases}$$

4th channel

$$\begin{cases} T^3R\cdot\exp[i\gamma(l_{11}+l_{21}+l_{31}+l_{41})]\exp[i(\varphi+3\psi)], \\ T^4R\cdot\exp[i\gamma(l_{12}+l_{22}+l_{32}+l_{42})]\exp[i(\varphi+4\psi)], \\ T^5R\cdot\exp[i\gamma(l_{13}+l_{23}+l_{33}+l_{43})]\exp[i(\varphi+5\psi)], \\ T^6R\cdot\exp[i\gamma(l_{14}+l_{24}+l_{34}+l_{44})]\exp[i(\varphi+6\psi)], \end{cases}$$

where $\gamma=\beta-i\alpha$ is the propagation constant of delay lines, l_{mn} is the length of the delay line from the nth DC of the mth channel to the nth transmitter or to the nth DC of the $(m+1)$th channel, $\varphi=\beta l_0+\pi/2$ is the phase of the DC coupling coefficient, $\psi=\beta l_0$ is the phase of the DC transmission coefficient, and βl_0 is the electric DC length.

From these expressions it follows that for small losses in the delay lines, the amplitude-phase distribution in the MAA transmitters is mainly determined by the DC parameters. The value of the coupling coefficient does not influence the pattern; however, the constant phase shift $\pi/2$ entering into the argument causes the pulse shape to distort. The phase shift (the delay time) acquired from the mth input to the nth transmitter is determined by the total electric length l_Σ of all delay lines and all directional couplers passed by the pulse. If the transmitters are spaced at distance d, the position of the pattern maximum θ_0 is specified by the relationship $d\cos\theta_0=c\tau$, where the angle θ_0 is counted from the array axis, τ is the time delay of pulses arriving at the neighboring transmitters, and c is the velocity of light. In order that the maximum of the beam corresponding to the mth input was in the direction θ_{0m}, the delay from the mth input to the nth transmitter must be $\tau_{mn}=(nd\cos\theta_{0m})/c$. Figure 2 shows the calculated shape of the input pulse together with the

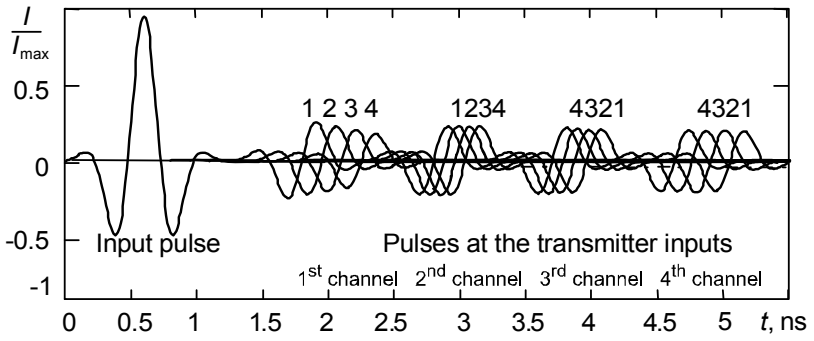

Fig. 2. Calculated time delays of pulses at the transmitter inputs for $d = 4$ cm, $\theta_{01} = 135°$, $\theta_{02} = 105°$, $\theta_{03} = 75°$, and $\theta_{04} = 45°$.

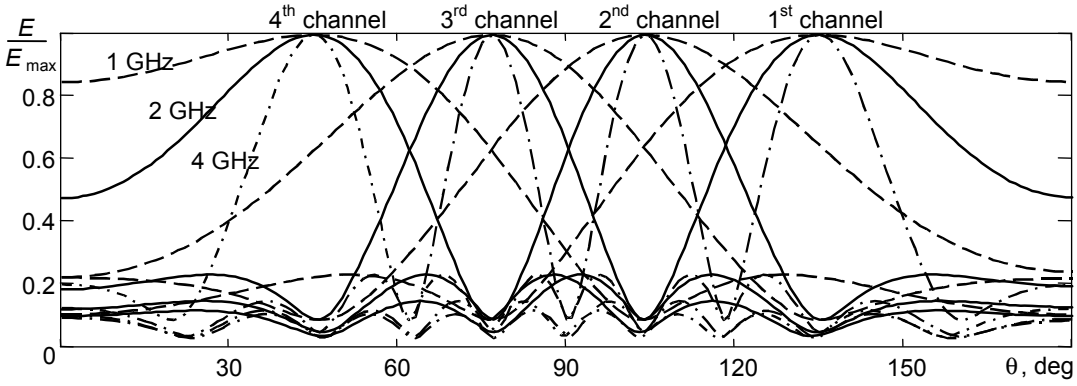

Fig. 3. Patterns corresponding to MAA channels at frequencies of 1 (dashed curves), 2 (solid curves), and 4 GHz (dot-dash curves).

time distribution of pulses at inputs of the transmitters of each channel. The duration of the pulse applied to the MAA inputs is about 0.5 ns, and its spectrum occupies the continuous frequency band with $f_{max} / f_{min} = 7$.

The patterns for the indicated delays are shown in Fig. 3. The solid curve here shows the pattern calculated for the average frequency of the pulse spectrum $f = 2$ GHz, and the dashed and dot-dash curves illustrate the patterns for frequencies of 1 and 4 GHz, respectively.

Results of calculations demonstrated that the MAA based on the Blass matrix allow several patterns to be formed with frequency-independent positions of their maxima using the directional couplers whose parameters are close to those of the ideal directional coupler.

ULTRA-WIDEBAND DIRECTIONAL COUPLER

Since the MAA characteristics are mainly determined by the parameters of the directional couplers used in the PFC, the possibility of developing the directional coupler with constant amplitude-frequency and linear phase-frequency characteristics in the frequency band of about three octaves was investigated. For the ideal DC, the elements of the scattering matrix have the following forms [5, 6]:

$$S_{11} = S_{22} = S_{33} = S_{44} = 0\,,\ S_{14} = S_{41} = S_{23} = S_{32} = 0\,,$$

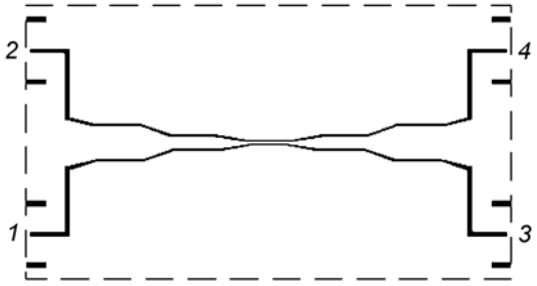

Fig. 4. Topology of the directional coupler comprising input *1*, coupling channel *2*, direct channel *3*, and decoupling channel *4*.

$$S_{12} = S_{21} = S_{34} = S_{43} = \frac{\sqrt{1-k^2}}{\sqrt{1-k^2}\cos\beta l + i\sin\beta l},\ S_{12} = S_{21} = S_{34} = S_{43} = \frac{ik\sin\beta l}{\sqrt{1-k^2}\cos\beta l + i\sin\beta l},$$

where $k = \dfrac{Z_{oe} - Z_{oo}}{Z_{oe} + Z_{oo}}$ is the coefficient of line coupling in voltage and $\beta l = \pi / 2$ is the electric length of the coupling segment. The DC matching condition is [6]

$$Z_{oe} Z_{oo} = Z_o^2,$$

where Z_{oe} is the wave impedance of even oscillations, Z_{oo} is the wave impedance of odd oscillations, and Z_o is the wave impedance of the loading line. The bandwidth of the ideal DC with $l = \pi/4$ reaches one octave if the DC dimensions are held to within 0.5%, where λ is the wavelength in the dielectric.

To extend the bandwidth, multicascade directional couplers are used representing a cascade connection of coupled line sections of the same lengths. For the coupling coefficient of the multicascade DC, the expression [6]

$$f(\beta l) = R\frac{4}{\pi}\left[w_1 \sin\beta l + w_2 \frac{\sin 3\beta l}{3} + ... + w_n \frac{\sin[(2n-1)\beta l]}{(2n-1)} \right]$$

is valid, where $R = 10^{-C/20}$ is the coupling coefficient; C is the transient attenuation of the directional coupler; w_1, w_2, ..., w_n are the weight functions (real constants) characterizing the wave impedances of each DC section, respectively; and n is the number of DC cascades.

A design of the three-cascade directional coupler with additional coupling elements was suggested in [7]; however, the DC bandwidth was smaller than two octaves. In this regard, the possibility was investigated of developing a microstrip directional coupler with a wider bandwidth using the printed circuit board technology and the method of etching. In this technology, the DC sizes can be held to within 50 μm; therefore, sizes of microstrips in calculations were set to within 0.1 mm. To reduce the overall DC dimensions, a foiled FLAN-10 dielectric was used. It was found impossible to provide the required relationship between Z_{oe} and Z_{oo} in the first and last cascades for the five-cascade microstrip DC having the theoretical bandwidth whose limiting frequencies were in the ratio $f_{\max} / f_{\min} = 7$; therefore, a dielectric layer was placed above the printed circuit board to increase the effective dielectric permittivity. The topology of the 60×40 mm five-cascade DC is shown in Fig. 4.

Results of calculations of the five-cascade DC shown in Fig. 5*a* demonstrate that for a preset accuracy of fabrication, the DC having the bandwidth with $f_{\max} / f_{\min} = 7$, coupling coefficient of $-(10 \pm 0.5)$ dB, reflection coefficient smaller than –20 dB, and decoupling coefficient no smaller than 25 dB can be developed. The experimental data (Fig. 5*b*) differ slightly from the theoretical ones, because we could not provide the required accuracy of prototype fabrication. Figure 6 shows the measured time characteristics of the directional coupler. Here curve *1* shows the test

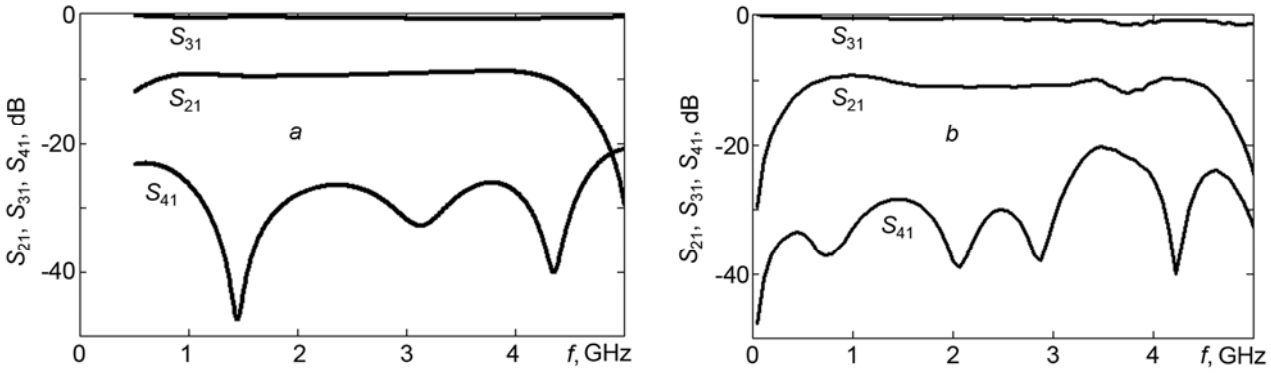

Fig. 5. Calculated (*a*) and experimental (*b*) characteristics of the directional coupler.

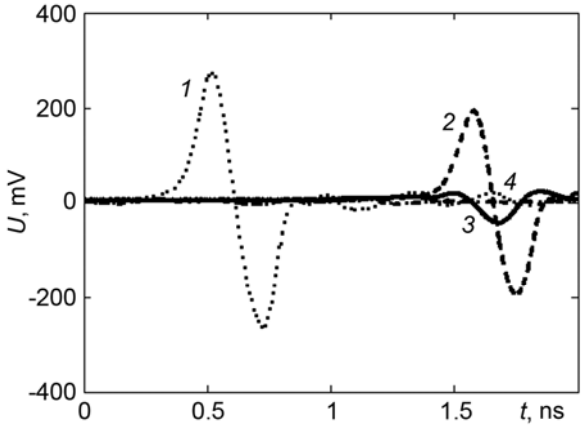

Fig. 6. Waveforms of the input (curve *1*), transitive (curve *2*), coupled (curve *3*), and decoupling pulses (curve *4*).

signal, curve *2* shows the transitive signal, curve *3* shows the coupling pulse, and curve *4* shows the decoupling pulse. From the figure it can be seen that the waveform of the coupling signal differs from that of the input signal.

A variant of the PFC topology based on five-cascade directional couplers is shown in Fig. 7. The suggested PFC design comprises two printed circuit boards with screens facing each other. All directional couplers and delay lines between the second and first channels and between the fourth and third channels are placed on one printed circuit board. The delay lines between the first channel and the transmitters and between the third and second channels are placed on the second printed circuit board. The DC printed circuit board is covered with the dielectric layer.

CONCLUSIONS

Based on our investigations, we can conclude that it is possible to develop a multibeam antenna array based on the Blass matrix and intended for generation of short ultra-wideband pulses. The transmitted pulse shape corresponds approximately to the second time derivative of the input pulse shape in the system. This is due to distortions induced by the directional coupler and pulse transmission by the UWB antennas. As a whole, this will lead to narrowing of the radiation spectrum.

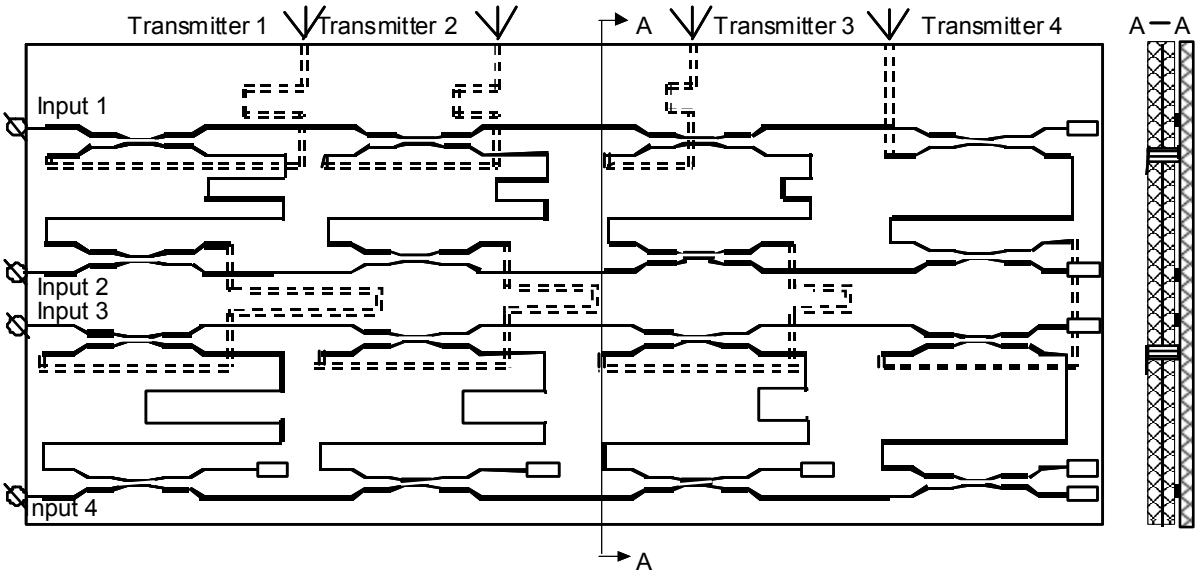

Fig. 7. Topology of the printed circuit board of the Blass matrix.

REFERENCES

1. D. I. Voskresenskii, Antennas and Microwave Devices [in Russian], Radio i Svyaz', Moscow (1994).
2. N. J. G. Fonseca, IEEE Trans. Antennas Propagat., **57**, No. 6, 1673–1677 (2009).
3. C.-C. Chang, R.-H. Lee, and T.-Y. Shih, IEEE Trans. Antennas Propagat., **58**, No. 2, 367–374 (2010).
4. V. S. Zvyagel'skii, S. D. Kremenetskii, V. F. Los', and M. T. Novosartov, Radiotekhnika, **34**, No. 7, 64–66 (1979).
5. A. L. Fel'dshtein, Radiotekh. Elektron., **4**, No. 2, 234–239 (1961).
6. R. K. Mongia, I. J. Bahl, P. Bhartia, and J. Hong, RF and Microwave Coupled-Line Circuits, Artech House, Boston (2007).
7. P. F. Shvadlenko, Yu. I. Buyanov, and V. I. Koshelev, in: Materials of the Conference "Materials Sciences, Technology, and Ecology in the 3rd Millennium MTE'2009" [in Russian], Tomsk (2009), pp. 48–52.